

From Dead Neurons to Deep Approximators: Deep Bernstein Networks as a Provable Alternative to Residual Layers

Ibrahim Albool¹ Malak Gamal El-Din¹ Salma Elmalaki¹ Yasser Shoukry¹

Abstract

Residual connections are the de facto standard for mitigating vanishing gradients, yet they impose structural constraints and fail to address the inherent inefficiencies of piecewise linear activations. We show that Deep Bernstein Networks (which utilizes Bernstein polynomials as activation functions) can act as residual-free architecture while simultaneously optimize trainability and representation power. We provide a two-fold theoretical foundation for our approach. First, we derive a theoretical lower bound on the local derivative, proving it remains strictly bounded away from zero. This directly addresses the root cause of gradient stagnation; empirically, our architecture reduces “dead” neurons from 90% in standard deep networks to less than 5%, outperforming ReLU, Leaky ReLU, SeLU, and GeLU. Second, we establish that the approximation error for Bernstein-based networks decays exponentially with depth, a significant improvement over the polynomial rates of ReLU-based architectures. By unifying these results, we demonstrate that Bernstein activations provide a superior mechanism for function approximation and signal flow. Our experiments on HIGGS and MNIST confirm that Deep Bernstein Networks achieve high-performance training without skip-connections, offering a principled path toward deep, residual-free architectures with enhanced expressive capacity.

1. Introduction

The unprecedented success of deep learning is fundamentally tied to our ability to optimize architectures of increasing depth. However, as networks grow deeper, they encounter severe optimization pathologies, most notably the vanishing gradient problem. To date, the machine learn-

ing community has largely relied on a structural remedy: the Residual Connection (He et al., 2016). While skip-connections have enabled the training of thousands of layers, they impose a rigid topological constraint—forcing the network to learn functions as incremental perturbations of the identity mapping—and do not resolve the underlying inefficiencies of the activation functions themselves. Piecewise linear activations like ReLU continue to suffer from the “dead neuron” phenomenon, which prunes network capacity, while smoother alternatives often lack rigorous guarantees for gradient preservation in the deep limit.

In this work, we propose a departure from these architectural *patches* in favor of an approach rooted in functional intrinsics. We investigate DeepBern-Nets, an architecture utilizing Bernstein polynomials as activation functions. While Bernstein-based layers have been introduced in preliminary contexts (Khedr & Shoukry, 2024), their theoretical properties regarding signal propagation and approximation efficiency in deep regimes have remained unexplored. We bridge this gap by stabilizing the DeepBern-Nets, introducing a framework that enforces strict domain constraints to satisfy basis requirements and ensure stable optimization.

Our contributions can be summarized as follows:

- **Guaranteed Trainability:** We derive a theoretical lower bound on the local Jacobian, proving that Bernstein derivatives remain strictly bounded away from zero. This safeguards the network against gradient collapse; empirically, we demonstrate a reduction in the “dead neuron” ratio from over 90% (in deep SELU and GeLU baselines) to less than 5% in our architecture.
- **Superior Expressivity:** We establish that the approximation error of DeepBern-Nets decays exponentially with depth at a rate of $\mathcal{O}(n^{-L})$. This fundamentally outperforms the established decay rates of ReLU networks (Yarotsky, 2018), suggesting that Bernstein-based neurons achieve higher *representational density*.
- **Residual-Free Performance:** Through extensive experiments on the HIGGS and MNIST datasets, we show that DeepBern-Nets are residual-free architecture that consistently matches or exceeds the performance of ResNet-style baselines.

¹Department of Electrical Engineering and Computer Science, University of California, Irvine, USA. Correspondence to: Ibrahim Albool <ialbool@uci.edu>.

2. Preliminaries

2.1. Bernstein Basis Polynomials

A polynomial of degree n can be represented in the Bernstein basis on an interval $[l, u]$ as $P_n^{[l,u]}(x) = \sum_{k=0}^n c_k b_{n,k}^{[l,u]}(x)$, where $c_k \in \mathbb{R}$ are the control coefficients. The Bernstein basis functions $b_{n,k}^{[l,u]}(x)$ are defined for $x \in [l, u]$ as:

$$b_{n,k}^{[l,u]}(x) = \frac{\binom{n}{k}}{(u-l)^n} (x-l)^k (u-x)^{n-k}, \quad (1)$$

where $\binom{n}{k}$ is the binomial coefficient. Unlike the power basis, the Bernstein representation is intrinsic to the domain $[l, u]$, meaning the coefficients c_k directly control the polynomial's geometry within this interval.

2.2. DeepBern-Nets

DeepBern-Nets (Khedr & Shoukry, 2024) are feed-forward neural networks where the standard activation functions are replaced by learnable Bernstein polynomials. For a network of depth L , we denote the input as $y^{(0)} = x$ and the output of the l -th layer as $y^{(l)}$. The propagation rule is given by:

$$y^{(l)} = \sigma \left(\mathbf{W}^{(l)} y^{(l-1)} + b^{(l)}; c^{(l)} \right), \quad (2)$$

where $\mathbf{W}^{(l)}$ and $b^{(l)}$ are the learnable weights and biases. The activation function σ operates element-wise, parametrized by a set of learnable Bernstein coefficients $c^{(l)} = \{c_k^{(l)}\}_{k=0}^n$. Specifically, for a pre-activation scalar input z , the activation is defined as:

$$\sigma(x; l, u, c^{(l)}) = \sum_{k=0}^n c_k^{(l)} b_{n,k}^{[l,u]}(x), \quad x \in [l, u]. \quad (3)$$

Here, n is a hyperparameter for the polynomial degree. This formulation allows the network to learn the shape of its non-linearities alongside its weights.

2.3. Stable training of DeepBern-Nets

Using polynomials as activation functions in deep NNs has attracted several researchers' attention in recent years (Wang et al., 2022; Gottemukkula, 2020). A major drawback of using polynomials of arbitrary order is their unstable behavior during training due to exploding gradients—which is prominent with the increase in order (Gottemukkula, 2020). Luckily, and thanks to the unique properties of Bernstein polynomials, DeepBern-Net does not suffer from such a limitation as captured in the next result (Khedr & Shoukry, 2024).

Proposition 2.1 (Khedr & Shoukry, 2024). *Consider the Bernstein activation function $\sigma(x; l, u, \mathbf{c})$ of arbitrary order n . The following holds:*

1. $|\sigma'(x; l, u, \mathbf{c})| \leq 2n \max_{k \in \{0, \dots, n\}} |c_k|$,
2. $|\sigma'(x; l, u, \mathbf{c})| \leq 1 \quad \text{for all } i \in \{0, \dots, n\}$.

Proposition 2.1 ensures that the gradient magnitude depends linearly on the learnable coefficients c_k , rather than exploding with high powers of the input x (as seen in monomial activations x^n for $x > 1$ (Gottemukkula, 2020)). This structural upper bound guarantees that training remains stable even in deep regimes. Furthermore, it implies that the Lipschitz constant of the network can be explicitly controlled by applying standard regularization (e.g., L_2 weight decay) to the coefficients c , directly penalizing large gradients.

3. Gradient Persistence: Theoretical Lower Bounds on Bernstein Derivatives

A core challenge in training deep, non-residual architectures is the degradation of signal propagation, often manifesting as a catastrophic increase in “dead” neurons. While standard activations like Leaky ReLU (Xu et al., 2015), Scaled Exponential ReLU (SeLU) (Klambauer et al., 2017) or Gaussian Error Linear Unit (GELU) (Hendrycks, 2016) offer various empirical advantages, they lack a functional form that guarantees local responsiveness across the entire input domain. In this section, we provide a formal analysis of the derivative properties of the Bernstein basis. We derive a theoretical lower bound for the local derivative of each neuron and demonstrate that, unlike piecewise linear or sigmoidal activations, Bernstein polynomials possess a unique “gradient-anchoring” property. This property ensures that the local Jacobian remains bounded away from zero, effectively preventing the vanishing gradient phenomenon. This theoretical foundation explains the dramatic reduction in inactive neurons observed in our experiments—dropping from 90% to 5%—and provides the mechanism for training deep networks without residual shortcuts.

3.1. Interval-Dependent Lower Bound

Before we show our result, we review the following properties of Bernstein polynomials.

Property 1 (Positivity (Titi, 2019)). Bernstein basis polynomials are non-negative on the interval $[l, u]$, i.e., $b_{n,k}^{[l,u]}(x) \geq 0$ for all $x \in [l, u]$.

Property 2 (Partition of Unity (Titi, 2019)). The sum of Bernstein basis polynomials of the same degree is equal to 1 on the interval $[l, u]$, i.e., $\sum_{k=0}^n b_{n,k}^{[l,u]}(x) = 1, \forall x \in [l, u]$.

Property 3 (Closed under differentiation (Doha et al., 2011)). The derivative of an n -degree Bernstein polynomial is n multiplied by the difference of two $(n-1)$ -degree Bernstein polynomials. Concretely:

$$\frac{d}{dx} b_{n,k}^{[l,u]}(x) = n \left(b_{n-1,k-1}^{[l,u]}(x) - b_{n-1,k}^{[l,u]}(x) \right)$$

Using these properties, we can now show the first result as follows:

Theorem 3.1 (Bernstein Gradient Lower Bound). *Let $\sigma(x; l, u, c)$ be a Bernstein activation of order n defined over $[l, u]$ with coefficients satisfying a strict monotonicity condition $|c_{k+1} - c_k| \geq \delta > 0$. The local derivative is bounded by:*

$$|\sigma'(x; l, u, c)| \geq \frac{n \cdot \delta}{u - l} \quad \forall x \in [l, u]. \quad (4)$$

Proof Sketch. Applying the chain rule to the standard Bernstein derivative yields another Bernstein polynomial (Property 3) with a scaling factor inversely proportional to the domain width. That is, the derivative of a Bernstein polynomial is a weighted sum of coefficient differences, scaled by the chain rule factor $\frac{d}{dx} \left(\frac{x-l}{u-l} \right) = \frac{1}{u-l}$. By the Positivity of Bernstein polynomials (Property 1) and the Partition of Unity (Property 2) of the Bernstein basis, the derivative is bounded by the minimum coefficient difference scaled by this factor. (See Appendix A for the full derivation).

Remarks:

- The lower bound in Theorem 3.1 is independent of the network depth L , ensuring that the local signal remains non-vanishing as $L \rightarrow \infty$.
- In ReLU-based architecture, a neuron that receives a negative pre-activation becomes “dead,” outputting a gradient of exactly 0 and effectively terminating the learning process for that path. Our result above shows that DeepBern-Nets ensures that the derivative is strictly positive, $\sigma'(x) > 0$, across the interval.
- By establishing a provable lower bound on the local derivative, we ensure that each layer acts as a reliable transducer of the gradient signal. In non-residual network architectures, the chain rule compounding of sub-unitary gradients leads to exponential decay; however, because our Bernstein coefficients are optimized to keep the local Jacobian bounded away from zero, the “gradient chain” remains robust.

3.2. Enforcing Non-Vanishing Flow in Deep Layers

While Theorem 3.1 guarantees non-vanishing gradients under the condition of strictly monotonic coefficients, enforcing this constraint during optimization is non-trivial. To achieve this target, we introduce the following architectural and parametrization changes.

3.2.1. THE NECESSITY OF BATCH NORMALIZATION

Equation 4 reveals a critical dependency: the gradient lower bound is inversely proportional to the per-neuron input range width $u - l$. In other words, if the input range $u - l$ is large, the gradient lower bound $\frac{n\delta}{u-l}$ approaches zero, re-introducing the vanishing gradient problem regardless of

the coefficient separation δ . Hence, to maximize the lower bound, we must minimize $u - l$ while ensuring the inputs fall within the support.

In other words, this theoretical insight necessitates the use of Batch Normalization to center and scale the pre-activations, ensuring that the vast majority of the signal mass falls within a fixed, narrow interval (e.g., $[-3, 3]$). This fixes $u - l$ to a small constant (e.g., 6), guaranteeing that the term $\frac{n\delta}{u-l}$ remains significant and the gradients remain *alive* throughout the network.

3.2.2. RE-PARAMETRIZATION OF BERNSTEIN LAYERS

In prior work (Khedr & Shoukry, 2024), the Bernstein polynomial coefficients c were treated as independent parameters, requiring complex projection steps. To strictly enforce the theoretical requirements of our gradient lower bound, we propose a *re-parameterization* of the Bernstein layer. Instead of learning the coefficients directly, we learn the base coefficient c_0 and a set of latent step parameters $\rho = \{\rho_0, \dots, \rho_{n-1}\}$.

Next, we define the k -th coefficient as a cumulative sum of positive increments enforced by a Softplus activation:

$$c_k = c_0 + \sum_{j=0}^{k-1} (\text{Softplus}(\rho_j) + \delta), \quad (5)$$

Algorithm 1 Stabilized Training Step for DeepBern-Nets

```

1: Input: Mini-batch  $\mathcal{X}$ , Targets  $t$ , Domain Bounds  $[l, u]$ 
2: Hyperparams: Learning rate  $\alpha$ , Degree  $n$ , Margin  $\delta$ 
3: Initialize:  $\rho \leftarrow \rho_{\text{init}}$  (Identity),  $c_0 \leftarrow 0$ 
4:  $y^{(0)} = \mathcal{X}$ 
5:  $\triangleright$  Forward Propagation
6: for  $i = 1$  to  $L$  do
7:    $z^{(i)} \leftarrow \mathbf{W}^{(i)} y^{(i-1)} + b^{(i)}$  {Linear Transformation}
8:    $\hat{z}^{(i)} \leftarrow \text{BatchNorm}(z^{(i)})$  {Mandatory for Bernstein stability}
9:    $\tilde{z}^{(i)} \leftarrow \text{Clamp}(\hat{z}^{(i)}, l, u)$  {Enforce Domain Condition}
10:  // Reconstruct monotonic coefficients from  $\rho$ 
11:  for  $k = 1$  to  $n$  do
12:     $c_k \leftarrow c_{k-1} + (\text{Softplus}(\rho_{k-1}) + \delta)$ 
13:  end for
14:   $y^{(i)} \leftarrow \sum_{k=0}^n c_k B_{k,n}(\tilde{z}^{(i)})$  {Evaluate Polynomial}
15:  end for
16:  $\triangleright$  Backpropagation
17:  $\text{Loss} \leftarrow \mathcal{L}(y^{(L)}, t)$ 
18: Compute gradients w.r.t.  $\mathbf{W}, b, c_0, \rho$ 
19:  $\rho \leftarrow \rho - \alpha \nabla_{\rho} \text{Loss}$  {Update latent step parameters}
20:  $\mathbf{W}, b, c_0 \leftarrow \text{Update}(\dots)$  {Weights, biases, coefficients}

```

where $\delta > 0$ is the fixed minimum margin derived in Theorem 3.1. By construction, this guarantees $c_{k+1} - c_k \geq \delta$, ensuring the activation satisfies the gradient lower bound condition throughout training.

Finally, to preserve signal variance at initialization, we solve for the parameters ρ such that the polynomial approximates the identity function $y = x$ over the normalized domain. We set:

$$\rho_{init} = \text{Softplus}^{-1} \left(\frac{1}{n} - \delta \right). \quad (6)$$

3.2.3. GRADIENT-ANCHORING TRAINING PROCEDURE.

Algorithm 1 details the training procedure. We enforce Batch Normalization to satisfy domain constraints $[l, u]$ and impose monotonicity via coefficient re-parameterization (Eq. 5), while leaving normalization optional for other layer types.

4. Superior Representation Power: DeepBern-Nets and the Convergence of Approximation Error

While gradient stability ensures that a network can be trained, the ultimate utility of an architecture is determined by its representation power—the efficiency with which it can approximate a target function given a fixed set of parameters. In this section, we analyze the approximation capabilities of DeepBern-Nets and prove that they possess a fundamental advantage over piecewise linear models. Specifically, we establish an upper bound on the approximation error that decays exponentially with the depth of the network L . Unlike ReLU-based architectures, which exhibit a slower rate of error reduction relative to depth, the Bernstein basis allows for a more compact representation of complex functions. By combining these faster convergence rates with the gradient persistence established in previous sections, we demonstrate that Bernstein networks are not only easier to optimize but are inherently more depth-efficient than their traditional counterparts.

4.1. Preliminaries: Modulus of Continuity

The approximation rate of any function approximator is fundamentally limited by the smoothness of the target function f . This is typically quantified using the *modulus of continuity* (De Vore & Lorentz, 1993; Dzyadyk & Shevchuk, 2008; Timan, 2014).

Definition 4.1 (Modulus of Continuity). Let $f : \Omega \rightarrow \mathbb{R}$ be a continuous function on a domain $\Omega \subset \mathbb{R}^d$. The modulus of continuity $\omega_f(\delta)$ is defined as the maximum fluctuation of f over any interval of size δ :

$$\omega_f(\delta) := \sup_{\substack{x, y \in \Omega \\ \|x - y\| \leq \delta}} |f(x) - f(y)|. \quad (7)$$

Intuitively, $\omega_f(\delta)$ measures how “wiggly” the function is. For Lipschitz continuous functions with constant K , then the modulus of continuity is bounded as $\omega_f(\delta) \leq K\delta$. The rate at which $\omega_f(\delta) \rightarrow 0$ as $\delta \rightarrow 0$ determines how quickly an estimator can converge to f .

4.2. Network Architecture and Algebraic Structure

To analyze the capacity of DeepBern-Nets, we explicitly derive the effective algebraic degree of the network. Let $\mathcal{N} : \mathbb{R}^d \rightarrow \mathbb{R}$ denote a feedforward neural network with depth L . We define the operation of the l -th layer as a composition of a linear transformation followed by a Bernstein polynomial activation.

Lemma 4.2 (Effective Degree of DeepBernNets). *Consider a DeepBern-Net of depth L , where every neuron computes a Bernstein polynomial of degree n . Assuming that for a given input \mathbf{x} , all intermediate pre-activations fall within the valid Bernstein support (e.g., via Batch Normalization), the output of the network $\mathcal{N}(\mathbf{x})$ is a multivariate polynomial of total degree D bounded by:*

$$D \leq n^L. \quad (8)$$

Proof. We proceed by induction on the depth L . *Base Case* ($L = 1$): The first layer computes $\sigma_n(\mathbf{W}^T \mathbf{x} + b)$. Since σ_n is a polynomial of degree n and the argument is linear in \mathbf{x} , the output is a polynomial of degree $n = n^1$.

Inductive Step: Assume the output of layer $l - 1$, denoted $h^{(l-1)}(\mathbf{x})$, consists of polynomials of total degree n^{l-1} . The l -th layer computes:

$$h^{(l)}(\mathbf{x}) = \sum_{k=0}^n c_k B_{n,k} \left(\mathcal{L}(h^{(l-1)}(\mathbf{x})) \right), \quad (9)$$

where \mathcal{L} is a linear map and $B_{n,k}$ denotes the Bernstein basis $b_{n,k}^{[l,u]}(\cdot)$. The basis function $B_{n,k}(\cdot)$ raises its input to the power n . Thus, the degree of the composition is the product of the degrees:

$$\deg(h^{(l)}) = n \cdot \deg(h^{(l-1)}) = n \cdot n^{l-1} = n^l. \quad (10)$$

By induction, the final output $\mathcal{N}(\mathbf{x})$ is a polynomial of degree n^L . \square

4.3. Approximation Bounds

We now leverage Jackson’s Inequality to bound the approximation error. To strictly isolate the benefit of depth, we analyze the capacity of the hypothesis space spanned by the network. While the exact set of polynomials representable by the network is a sub-manifold of the full polynomial space Π_{n^L} , we assume that for the target class of functions (e.g., compositional functions), the optimal approximator lies within the network’s capacity.

Assumption 4.3 (Sufficient Capacity). Let $f \in C(\mathbb{R}^d)$. We assume that the best polynomial approximation of f of degree n^L , denoted $P_{n^L}^*$, lies within the hypothesis space of the network \mathcal{N} . Specifically, there exists a parameter configuration θ^* such that $\mathcal{N}(x; \theta^*) = P_{n^L}^*(x)$.

Assumption 4.4 (Non-Choking Condition). To ensure the global validity of the layer-wise approximation, we assume the network width W is sufficiently large to prevent information bottlenecks. Specifically, we require $W \geq d$, where d is the dimension of the input manifold. As shown in (Kileel et al., 2019), this guarantees that the network possesses sufficient capacity to propagate the approximated features to the next layer without rank collapse, ensuring that the total error is dominated by the polynomial degree n and depth L .

Theorem 4.5 (Exponential Approximation Rate). *Let $f : \mathbb{R}^d \rightarrow \mathbb{R}$ be a continuous function satisfying Assumption 4.3. Then, there exists a DeepBern-Net \mathcal{N} of depth L and degree n such that:*

$$\|\mathcal{N} - f\|_\infty \leq C_d \cdot \omega_f \left(\frac{1}{n^L} \right), \quad (11)$$

where C_d is a constant that depends only on dimension d .

Proof. By Lemma 4.2, the network output $\mathcal{N}(x)$ resides in Π_{n^L} , the space of polynomials of total degree n^L . According to Jackson’s Theorem for multivariate polynomial approximation (DeVore & Lorentz, 1993), for any continuous function f , the error of the best polynomial approximation $P^* \in \Pi_D$ is bounded by:

$$\inf_{P \in \Pi_D} \|P - f\|_\infty \leq C_d \cdot \omega_f \left(\frac{1}{D} \right). \quad (12)$$

Setting $D = n^L$, let $P_{n^L}^*$ be the best approximating polynomial in the full space Π_{n^L} . Its error satisfies:

$$\|P_{n^L}^* - f\|_\infty \leq C_d \cdot \omega_f \left(\frac{1}{n^L} \right). \quad (13)$$

By Assumption 4.3, the specific polynomial $P_{n^L}^*$ lies within the realizable manifold of our neural network \mathcal{N} . Thus, the network’s optimal error coincides with the polynomial error:

$$\min_{\theta} \|\mathcal{N}(\cdot; \theta) - f\|_\infty \leq C_d \cdot \omega_f \left(\frac{1}{n^L} \right). \quad (14)$$

□

4.4. Comparison with SOTA Approximation Bounds

To contextualize the efficiency of DeepBern-Nets, we compare our derived bound against foundational results for ReLU networks and recent super-approximation architectures. Table 1 summarizes these rates for a continuous function f with modulus of continuity $\omega_f(\cdot)$. In the table, ReLU_{std} and ReLU_{opt} denote standard ReLU networks analyzed by Yarotsky (Yarotsky, 2018) and Shen et al. (Shen et al., 2022), respectively. ReLU_{flr} represents Floor-ReLU networks (Shen et al., 2021a), and FLES denotes Floor-Exponential-Step networks (Shen et al., 2021b).

Table 1. Comparison of approximation error bounds. ReLU_{std} : Yarotsky (Yarotsky, 2018); ReLU_{opt} : Shen et al. (Shen et al., 2022); ReLU_{flr} (Shen et al., 2021a); FLES (Shen et al., 2021b).

METHOD	WIDTH	DEPTH	ERROR RATE
ReLU_{std}	$\mathcal{O}(W)$	$\mathcal{O}(L)$	$\omega_f \left((W^2 L^2)^{-1/d} \right)$
ReLU_{opt}	$\mathcal{O}(W)$	$\mathcal{O}(L)$	$\omega_f \left((W^2 L^2 \ln W)^{-1/d} \right)$
ReLU_{flr}	$\mathcal{O}(W)$	$\mathcal{O}(L)$	$\omega_f \left(W^{-\sqrt{L}} \right)$
FLES	$\mathcal{O}(W)$	3	$\omega_f \left(2^{-W} \right) + \mathcal{O}(2^{-W})$
DEEPBERN-NETS	$\mathcal{O}(W)$	$\mathcal{O}(L)$	$\omega_f \left(n^{-L} \right)$

Standard ReLU networks are inherently limited by a polynomial decay in error. Yarotsky (Yarotsky, 2018) established that for a network of width W and depth L , the error scales as $\omega_f((W^2 L^2)^{-1/d})$. Even with the optimized constants derived by Shen et al. (Shen et al., 2022), the fundamental polynomial rate remains unchanged. This implies that doubling the depth yields only a marginal reduction in approximation error, making high-precision approximation prohibitively expensive in terms of parameter count.

To overcome this polynomial barrier, architectures such as ReLU_{flr} and FLES introduce non-differentiable operators. As shown in Table 1, utilizing the floor or step functions allows these networks to achieve root-exponential or exponential convergence rates, such as $\omega_f(2^{-W})$. However, the reliance on operators that have zero gradients almost everywhere renders these architectures unsuitable for standard gradient-based optimization, creating a gap between theoretical capacity and practical trainability.

DeepBern-Nets bridge this gap by achieving an exponential approximation rate of $\mathcal{O}(\omega_f(n^{-L}))$ purely through depth. Mathematically, the term n^{-L} decays significantly faster than the polynomial factor $L^{-2/d}$ associated with standard ReLU networks. Crucially, unlike the super-approximation methods that rely on discontinuous functions, we achieve this rate using strictly differentiable Bernstein polynomials. This ensures that the network retains the high theoretical capacity of super-approximators while remaining amenable to efficient training via backpropagation.

5. Results and Discussion

In this section, we empirically validate the theoretical properties of DeepBern-Nets, focusing on the strict lower bound on local derivatives (Theorem 3.1) and the resulting gradient dynamics in deep networks. We evaluate our method against standard baselines on two distinct modalities: the **HIGGS** dataset (dense physics simulation data) and **MNIST** (image classification). Unless otherwise stated, all experiments utilize a Fully Connected Network (FCN) architecture with depth $L = 50$ and width $W = 100$.

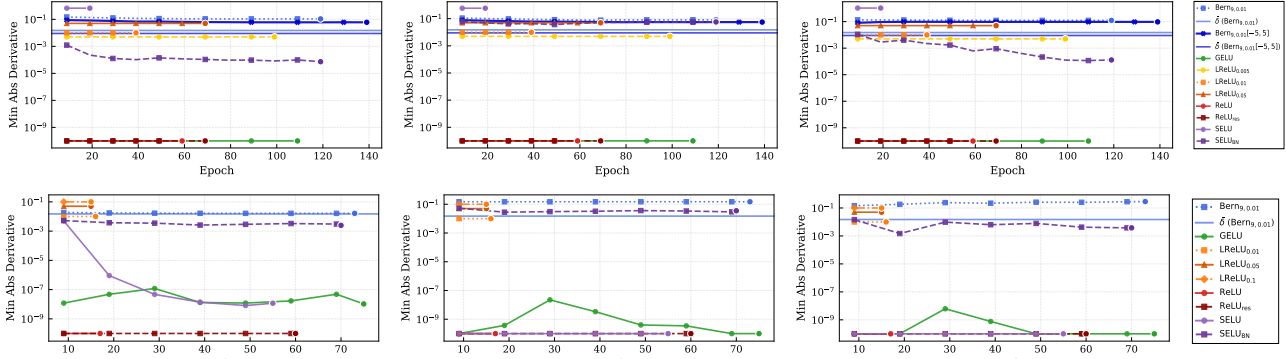


Figure 1. Minimum absolute derivative across training epochs at layers 1 (left), 25 (middle), and 50 (right) using HIGGS dataset (Top) and MNIST dataset (Bottom). The theoretical lower bound $\bar{\delta}$ is shown for Bernstein polynomial activations.

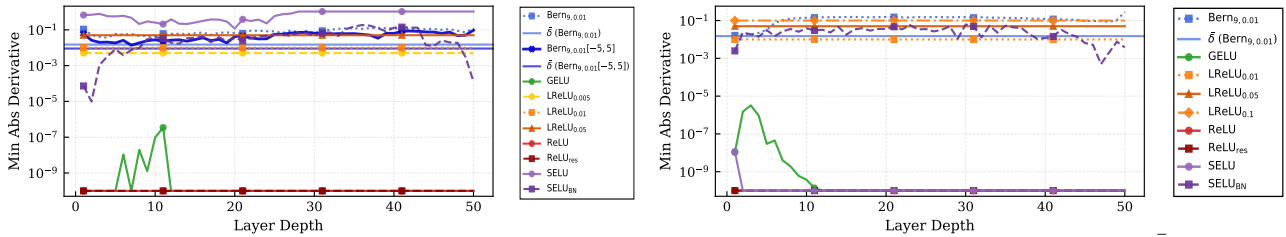


Figure 2. Minimum absolute derivative across network depth at the final training epoch. The theoretical lower bound $\bar{\delta}$ is shown for Bernstein polynomial activations. (Left) HIGGS dataset and (Right) MNIST dataset.

5.1. Experimental Setup

We compare DeepBern-Nets against a comprehensive suite of baselines: ReLU, Residual ReLU (ReLU_{res}), GELU, SELU without Batch Normalization (SELU), SELU with Batch Normalization (SELU_{BN}), and Leaky ReLU (LReLU) with leak coefficients $\{0.005, 0.01, 0.05, 0.1\}$ denoted as LReLU_{0.005}, LReLU_{0.01}, and LReLU_{0.05}, respectively. For DeepBern-Nets, we evaluate polynomial orders $n \in \{9, 15\}$ and intervals $[l, u] \in \{[-3, 3], [-5, 5]\}$ with strict monotonicity margins $\delta \in \{0.005, 0.01, 0.05\}$. We use $\text{Bern}_{n,\delta}$ and $\text{Bern}_{n,\delta}[-5, 5]$ to denote these networks as for various values of δ and n .

Training Protocol. All models were trained using the AdamW optimizer. Batch Normalization (BN) was applied to all activations except SELU (where we test both configurations).

- **HIGGS (1.1×10^7 samples):** We utilized an 80%/20% training-validation split. Training used batch size 2048, initial learning rate (LR) 1.0×10^{-4} , and weight decay 1.0×10^{-4} starting at epoch 5. We used ReduceLROnPlateau monitoring AUC, with early stopping triggered after 20 epochs of no improvement ($\Delta < 10^{-4}$).

- **MNIST (70,000 samples):** We utilized a 60k/10k training-validation split. Training used batch size 64, initial LR 2.0×10^{-3} , and weight decay 1.0×10^{-4} . We used an exponential LR decay ($\gamma = 0.95$) starting at epoch 5. Early stopping was set to 15 epochs monitoring test accuracy ($\Delta < 10^{-3}$).

5.2. Experiment 1: Analysis of Local Derivative Lower Bounds in Theorem 3.1

We first investigate the local behavior of the activation functions. According to Theorem 3.1, the derivative of the Bernstein activation is strictly bounded by $\bar{\delta} = \frac{n \cdot \delta}{u - l}$. We visualize the minimum absolute derivative $|\sigma'(x)|$ observed during training to confirm this guarantee.

5.2.1. TEMPORAL EVOLUTION OF LOCAL DERIVATIVES

We first examine the stability of gradients throughout the optimization process. Figure 1 illustrates the minimum absolute derivative $|\sigma'(z)|$ tracked across training epochs for both the HIGGS and MNIST datasets.

- **Theoretical Adherence:** For DeepBern-Nets ($n = 9, \delta = 0.01$), we tested two operational intervals: $[-3, 3]$ and $[-5, 5]$, with corresponding theoretical bounds of $\bar{\delta} \approx 0.015$ and $\bar{\delta} \approx 0.009$, respectively. Across both datasets and all layers (early, middle, and deep), the empirical derivatives consistently respect these lower bounds derived in Theorem 3.1.

- **Baselines Collapse:** In stark contrast, standard activations such as ReLU, GeLU, and even Res-ReLU demonstrate catastrophic gradient decay, with minimum derivatives vanishing to near-zero ($< 10^{-9}$) within the first few epochs. While LReLU maintains a non-zero gradient, its “leak” is a static hyperparameter; DeepBern, conversely, dynamically learns steeper, more expressive gradients while using the bound only as a safety floor.

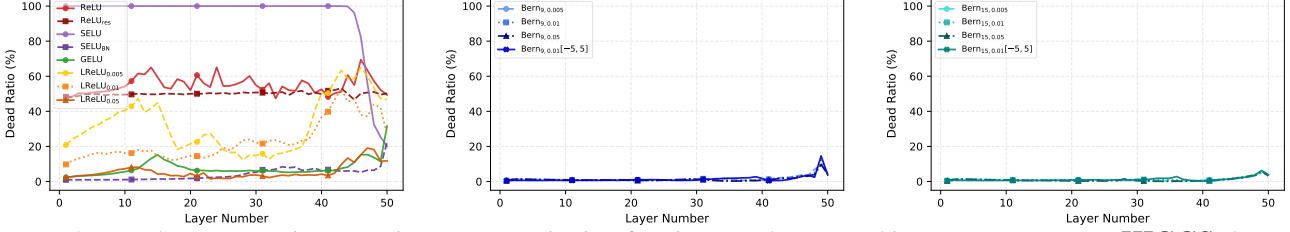


Figure 3. Dead Neuron Ratio comparison across activation functions on the NN architecture 100×50 on **HIGGS** dataset with the activation functions: ReLU, ReLU_{res} , SELU, SELU_{BN} , GELU, $\text{LReLU}_{0.005}$, $\text{LReLU}_{0.01}$, $\text{LReLU}_{0.05}$ against (left) $\text{Bern}_{9,0.01}[-5, 5]$, $\text{Bern}_{15,0.01}[-5, 5]$, (middle) $\text{Bern}_{9,0.005}$, $\text{Bern}_{9,0.01}$, $\text{Bern}_{9,0.05}$, $\text{Bern}_{9,0.01}[-5, 5]$, and (right) $\text{Bern}_{15,0.005}$, $\text{Bern}_{15,0.01}$, $\text{Bern}_{15,0.05}$, $\text{Bern}_{15,0.01}[-5, 5]$. The y-axis shows the average dead neuron percentage over the last epoch for a layer in logarithmic scale vs. the layer number.

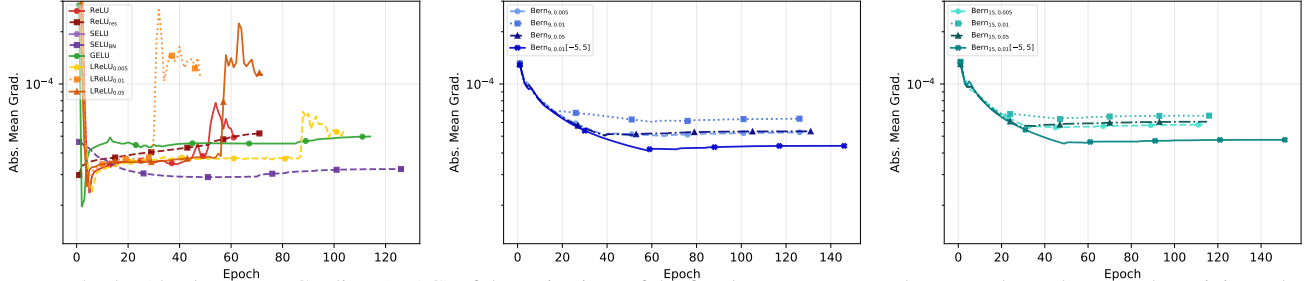


Figure 4. The Absolute Mean Gradient (MAG) of the activations of the first layer over an epoch vs. epoch number over the training. The comparison across activation functions on the NN architecture 100×50 for the dataset **HIGGS** with the activation functions: ReLU, ReLU_{res} , SELU, SELU_{BN} , GELU, $\text{LReLU}_{0.005}$, $\text{LReLU}_{0.01}$, $\text{LReLU}_{0.05}$ against (left) $\text{Bern}_{9,0.01}[-5, 5]$, $\text{Bern}_{15,0.01}[-5, 5]$, (middle) $\text{Bern}_{9,0.005}$, $\text{Bern}_{9,0.01}$, $\text{Bern}_{9,0.05}$, $\text{Bern}_{9,0.01}[-5, 5]$, and (right) $\text{Bern}_{15,0.005}$, $\text{Bern}_{15,0.01}$, $\text{Bern}_{15,0.05}$, $\text{Bern}_{15,0.01}[-5, 5]$. The y-axis is in logarithmic scale.

5.2.2. DERIVATIVE CONSISTENCY VS NETWORK DEPTH

To investigate the “vanishing” phenomenon in the spatial dimension, we analyze the profile of minimum derivatives across all 50 layers (Figure 2).

- **Vanishing vs. Persistence:** In standard non-residual configurations, ReLU and GeLU show a complete collapse of local derivatives as depth increases, effectively “killing” signal propagation in deeper layers.
- **Stability and Variance:** While SELU (paired with Batch Normalization) manages to avoid total collapse, it exhibits high variance and significant fluctuations across the network’s depth. Our DeepBern-Nets architecture maintains a markedly smoother and more consistent derivative profile. This stability suggests that Bernstein activations provide a more controlled optimization landscape.
- **Interval Trade-offs:** The results across HIGGS and MNIST confirm that while a wider interval ($[-5, 5]$) leads to a theoretically tighter (lower) bound, it still preserves a healthier gradient flow than standard baselines, proving that the Bernstein basis is robust to different scaling configurations.

5.3. Experiment 2: Gradient Dynamics and Network Sparsity

While local derivatives ensure individual neuron health, we now evaluate how these properties scale to global training dynamics. We employ two diagnostic metrics: (1) the **Dead**

Neuron Ratio, defined as the fraction of neurons with an absolute gradient below 10^{-7} , representing “closed” flow paths; and (2) the **Mean Absolute Gradient (MAG)** of the first layer, which quantifies the total learning signal surviving the backpropagation through the full depth of the network.

5.3.1. NETWORK CONNECTIVITY AND GATE STABILITY

The dead neuron ratio provides a snapshot of the network’s functional width. As shown in Figures 3 and 5 across both HIGGS and MNIST datasets, DeepBern-Nets demonstrate a high degree of connectivity that baseline architectures fail to match.

- **Sustained Transparency:** DeepBern-Nets architectures maintain a remarkably consistent and low dead ratio ($< 5\%$) across almost all layers. The smooth profile suggests that “gradient gates” remain open, ensuring that nearly the entire width of the network participates in feature learning.
- **The Baseline Clog:** In contrast, non-residual baselines suffer from severe pathologies. SELU (without Batch Normalization) exhibits a catastrophic 100% dead ratio across the majority of the network, effectively severing the learning signal. Even Residual ReLU, which bypasses these gates via shortcuts, still reports a $\approx 50\%$ dead ratio, indicating significant under-utilization of the network’s capacity.

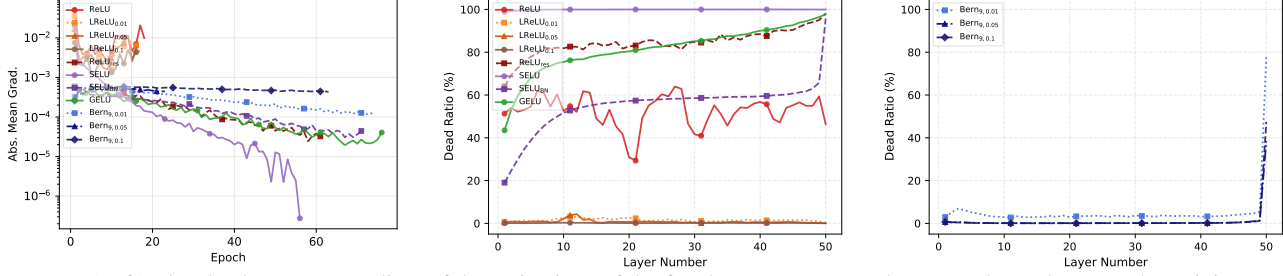


Figure 5. (Left) The absolute mean gradient of the activations of the first layer over an epoch vs. epoch number over the training. For MNIST Dead ratio comparison for non-Bernstein activations (Middle) and Bernstein activations (Right).

- **Volatility in ReLU variants:** While Leaky ReLU reduces the absolute number of dead neurons, it introduces high-frequency fluctuations (“wiggling”) across layers, destabilizing the optimization landscape. DeepBern-Nets avoids this volatility, providing a predictable and stable trajectory throughout the training process as visualized in our heatmap analysis (Appendix C).

5.3.2. ROBUSTNESS OF THE BACKPROPAGATION SIGNAL

The Mean Absolute Gradient (MAG) serves as a proxy for the health of the *long-range* gradient signal. Figure 4 (HIGGS) and Figure 5 (MNIST) illustrate the MAG of the first layer as it relates to training epochs.

- **Smooth Signal Decay:** Both Order 9 and 15 DeepBern-Nets models exhibit a smooth, controlled decay of the gradient as training converges. Unlike ReLU and Leaky ReLU, which display massive volatility and spikes during learning rate shifts (epochs 30 and 55), DeepBern-Nets remains robust to scheduler jumps.
- **Signal Magnitude:** While SELU-BN maintains smoothness, its signal strength is orders of magnitude weaker ($\approx 2 \times 10^{-5}$), bordering on the vanishing regime. DeepBern-Nets maintains a significantly stronger signal, facilitating faster and more reliable convergence.

5.4. Experiment 3: Scaling and Compressibility

Having demonstrated that DeepBern-Nets are easier to optimize, we now evaluate their representational efficiency. According to Theorem 4.5, the approximation error of these networks scales at a rate superior to that of ReLU-based models. This section empirically tests the hypothesis that the higher-order Bernstein basis can achieve equivalent or superior function approximation with significantly less architectural depth.

5.4.1. DEPTH COMPRESSION VS COMPLEXITY SCALING

To test the spectral scaling property of our architecture, we established a baseline using a standard 50-layer ReLU network ($W = 100$). We then compared this against progressively shallower DeepBern-Nets configurations.

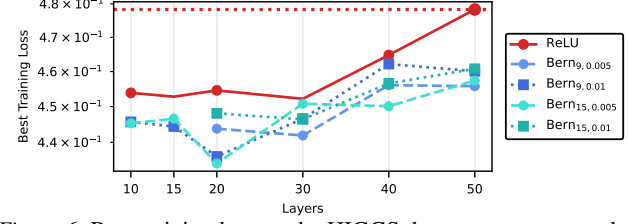


Figure 6. Best training loss on the HIGGS dataset versus network depth for ReLU and Bernstein networks. The x-axis represents the number of layers of size 100 neurons. We compare against the baseline relu horizontal line with 50 layers.

- **Compression Advantage:** As illustrated in Figure 6, DeepBern-Nets architectures ($n = 10, 15$) consistently achieved a lower training loss than the full-depth ReLU baseline. Remarkably, even when the DeepBern-Nets network was compressed to just $L = 10$ layers—a five-fold reduction in depth—it still outperformed the 50-layer ReLU network. This confirms that Bernstein polynomials can capture complex, high-frequency kinematic functions (as seen in the HIGGS dataset) more compactly than the piecewise linear “bent-line” approximations of ReLU.
- **Robustness to Pruning:** In a reduced-width regime (50×50), DeepBern-Nets ($n = 15$) maintained its edge, achieving superior training loss compared to much wider ReLU baselines. This suggests that the expressive power of the Bernstein basis is robust to both depth and width pruning.

5.4.2. SHALLOW EXPRESSIVITY ON MNIST

The advantage of the Bernstein basis is even more pronounced in discrete classification tasks. Table 2 (Appendix D) summarizes the ablation study on MNIST:

- **Single-Layer Parity:** A single-hidden-layer DeepBern-Nets network ($n = 9$) achieved a training loss of 0.0003. This performance matches the accuracy that ReLU networks only achieved after stacking multiple deep layers.
- **Capacity Density:** These results suggest that the *capacity per parameter* is significantly higher in Bernstein-based neurons, allowing for high-performance training in shallow regimes where traditional activations struggle with underfitting.

Impact Statement

This paper presents a foundational advance in the design of deep neural networks by moving beyond piecewise linear activations. The primary impact of this work lies in computational efficiency and sustainability. By establishing that DeepBern-Nets achieve exponential approximation rates $\mathcal{O}(n^{-L})$, we demonstrate that high-accuracy models can be constructed with significantly fewer parameters and layers than standard ReLU networks. This "spectral compression" has direct implications for Green AI, potentially reducing the energy consumption required for training and inference, and facilitating deployment on resource-constrained edge devices. Furthermore, the smoothness of Bernstein approximations offers particular utility in the natural sciences, as evidenced by our results on high-energy physics datasets (HIGGS), where modeling smooth kinematic functions is critical. We do not foresee immediate negative societal consequences beyond the general dual-use risks inherent to deep learning technologies.

Acknowledgment

This work was partially supported by the NSF award CNS #2504809 and the UCI ProperAI Institute, an Engineering+Society Institute funded as part of a generous gift from Susan and Henry Samueli

References

DeVore, R. A. and Lorentz, G. G. *Constructive approximation*, volume 303. Springer Science & Business Media, 1993.

Doha, E., Bhrawy, A., and Saker, M. On the derivatives of bernstein polynomials: an application for the solution of high even-order differential equations. *Boundary Value Problems*, 2011:1–16, 2011.

Dzyadyk, V. K. and Shevchuk, I. A. *Theory of uniform approximation of functions by polynomials*. Walter de Gruyter, 2008.

Gottemukkula, V. Polynomial activation functions. 2020.

He, K., Zhang, X., Ren, S., and Sun, J. Deep residual learning for image recognition. In *Proceedings of the IEEE conference on computer vision and pattern recognition*, pp. 770–778, 2016.

Hendrycks, D. Gaussian error linear units (gelus). *arXiv preprint arXiv:1606.08415*, 2016.

Khedr, H. and Shoukry, Y. Deepbern-nets: Taming the complexity of certifying neural networks using bernstein polynomial activations and precise bound propagation. In *Proceedings of the AAAI Conference on Artificial Intelligence*, volume 38, pp. 21232–21240, 2024.

Kileel, J., Trager, M., and Bruna, J. On the expressive power of deep polynomial neural networks. *Advances in neural information processing systems*, 32, 2019.

Klambauer, G., Unterthiner, T., Mayr, A., and Hochreiter, S. Self-normalizing neural networks. *Advances in neural information processing systems*, 30, 2017.

Shen, Z., Yang, H., and Zhang, S. Deep network with approximation error being reciprocal of width to power of square root of depth. *Neural Computation*, 33(4):1005–1036, 2021a.

Shen, Z., Yang, H., and Zhang, S. Neural network approximation: Three hidden layers are enough. *Neural Networks*, 141:160–173, 2021b.

Shen, Z., Yang, H., and Zhang, S. Optimal approximation rate of relu networks in terms of width and depth. *Journal de Mathématiques Pures et Appliquées*, 157:101–135, 2022.

Timan, A. F. *Theory of approximation of functions of a real variable*, volume 34. Elsevier, 2014.

Titi, J. *Matrix Methods for the Tensorial and Simplicial Bernstein Forms with Application to Global Optimization*. PhD thesis, 01 2019.

Wang, J., Chen, L., and Ng, C. W. W. A new class of polynomial activation functions of deep learning for precipitation forecasting. In *Proceedings of the Fifteenth ACM International Conference on Web Search and Data Mining*, WSDM '22, pp. 1025–1035, New York, NY, USA, 2022. Association for Computing Machinery. ISBN 9781450391320. doi: 10.1145/3488560.3498448. URL <https://doi.org/10.1145/3488560.3498448>.

Xu, B., Wang, N., Chen, T., and Li, M. Empirical evaluation of rectified activations in convolutional network. *arXiv preprint arXiv:1505.00853*, 2015.

Yarotsky, D. Optimal approximation of continuous functions by very deep relu networks. In *Conference on learning theory*, pp. 639–649. PMLR, 2018.

A. Proofs of Trainability

In this section, we provide the rigorous derivation of the gradient lower bounds presented in Section 3. We explicitly account for the domain scaling factor $\frac{1}{u-l}$, which motivates the normalization strategies discussed in the main text.

A.1. Derivative of Bernstein Polynomials on Arbitrary Intervals

Lemma A.1 (Bernstein Derivative Formula). *Let $B_n(x; \mathbf{c})$ be a Bernstein polynomial of degree n defined on $[l, u]$ with coefficients $\mathbf{c} = \{c_0, \dots, c_n\}$. Its derivative with respect to x is:*

$$\frac{d}{dx} B_n(x) = \frac{n}{u-l} \sum_{k=0}^{n-1} (c_{k+1} - c_k) b_{k,n-1} \left(\frac{x-l}{u-l} \right), \quad (15)$$

where $b_{k,m}(t) = \binom{m}{k} t^k (1-t)^{m-k}$ are the standard Bernstein basis polynomials on $[0, 1]$.

Proof. Let $t = \frac{x-l}{u-l}$. By the chain rule, $\frac{d}{dx} = \frac{dt}{dx} \frac{d}{dt} = \frac{1}{u-l} \frac{d}{dt}$. The derivative of a standard Bernstein polynomial with respect to t is known to be $n \sum_{k=0}^{n-1} (c_{k+1} - c_k) b_{k,n-1}(t)$. Multiplying by the scaling factor $\frac{1}{u-l}$ yields the result. \square

A.2. Element-wise Derivative Bounds

We now define the rigorous bounds for a single neuron's activation derivative based on its coefficients.

Lemma A.2 (Bounds on Local Derivative). *For a neuron with interval $[l, u]$ and coefficients \mathbf{c} , define the scaled minimum and maximum differences:*

$$\underline{m} = \frac{n}{u-l} \min_k (c_{k+1} - c_k), \quad \overline{m} = \frac{n}{u-l} \max_k (c_{k+1} - c_k). \quad (16)$$

Then, for all $x \in [l, u]$, the derivative $\sigma'(x)$ satisfies:

$$\underline{m} \leq \sigma'(x) \leq \overline{m}. \quad (17)$$

Proof. From the lemma above, $\sigma'(x) = \frac{n}{u-l} \sum_{k=0}^{n-1} (c_{k+1} - c_k) b_{k,n-1}(t)$. The Bernstein basis functions form a partition of unity, meaning $b_{k,n-1}(t) \geq 0$ and $\sum_{k=0}^{n-1} b_{k,n-1}(t) = 1$ for $t \in [0, 1]$. Therefore, $\sigma'(x)$ is a convex combination (weighted average) of the terms $\frac{n}{u-l} (c_{k+1} - c_k)$. The value of a convex combination is always bounded by the minimum and maximum elements of the set. Thus, $\underline{m} \leq \sigma'(x) \leq \overline{m}$. \square

A.3. Uniform Diagonal Lower Bounds (The Main Theorem)

Theorem A.3 (Sign-robust uniform diagonal bound). *Fix a layer r . Let $\underline{m}_k^{(r)}$ and $\overline{m}_k^{(r)}$ be defined as in Lemma A.2. If there exists a step size $\delta > 0$ such that for all neurons $k = 1, \dots, d_r$, either*

$$\underline{m}_k^{(r)} \geq \frac{n\delta}{u-l}, \quad (18)$$

or

$$\overline{m}_k^{(r)} \leq -\frac{n\delta}{u-l}. \quad (19)$$

Then, defining $|D^{(r)}(x^{(r)})|$ as the diagonal matrix of element-wise absolute derivatives, i.e.,

$$|D^{(r)}(x^{(r)})|_{ii} := |\sigma'_i(x_i^{(r)})|, \quad (20)$$

we have the following matrix inequality for all admissible pre-activations $x^{(r)}$:

$$|D^{(r)}(x^{(r)})| \succeq \frac{n\delta}{u-l} I_{d_r}. \quad (21)$$

Proof. Fix any neuron k . If condition (18) holds, then by Lemma A.2:

$$\sigma'_k(x) \geq \underline{m}_k \geq \frac{n\delta}{u-l} \implies |\sigma'_k(x)| \geq \frac{n\delta}{u-l}.$$

If condition (19) holds, then:

$$\sigma'_k(x) \leq \bar{m}_k \leq -\frac{n\delta}{u-l} \implies |\sigma'_k(x)| \geq \frac{n\delta}{u-l}.$$

Since $|D^{(r)}|$ is a diagonal matrix containing these absolute values on the diagonal, and every diagonal entry is at least $\frac{n\delta}{u-l}$, it follows that $|D^{(r)}| \succeq \frac{n\delta}{u-l} I$. \square

Corollary A.4 (Strict Monotonicity). *Under the assumptions of Theorem A.3, each activation function is strictly monotone on $[l, u]$. Specifically, the derivative never changes sign and is bounded away from zero by $\frac{n\delta}{u-l}$, ensuring no signal stagnation occurs within the domain.*

B. Extension of Theorem 4.5 to Vector-Valued Functions

In this section, we formally extend the approximation results of Theorem 4.5 to vector-valued functions $f : \mathbb{R}^d \rightarrow \mathbb{R}^m$.

Corollary B.1 (Vector-Valued Approximation). *Let $f = (f_1, \dots, f_m)^T$ be a continuous function from \mathbb{R}^d to \mathbb{R}^m . Assume each component function f_j satisfies the capacity Assumption 4.3. Then, there exists a DeepBern-Net $\mathcal{N} : \mathbb{R}^d \rightarrow \mathbb{R}^m$ of depth L and degree n such that:*

$$\|\mathcal{N} - f\|_{\infty, \text{vec}} \leq C_d \cdot \max_{j=1, \dots, m} \omega\left(f_j, \frac{1}{n^L}\right), \quad (22)$$

where $\|\mathbf{g}\|_{\infty, \text{vec}} := \sup_x \max_j |g_j(x)|$.

Proof. Let the target function be $f(x) = [f_1(x), \dots, f_m(x)]^T$. A DeepBern-Net with m outputs can be written as $\mathcal{N}(x) = [\mathcal{N}_1(x), \dots, \mathcal{N}_m(x)]^T$, where each $\mathcal{N}_j(x)$ shares the same hidden layers (feature extractor) but has a distinct set of weights in the final linear layer.

However, to prove existence, we can construct a network where the parameters are not necessarily shared, or simply view the optimization of the final layer weights as independent problems given a sufficiently rich feature basis. More conservatively, we can invoke the scalar existence theorem (Theorem 4.5) for each component independently.

For each output dimension $j \in \{1, \dots, m\}$, Theorem 4.5 guarantees the existence of a polynomial (and thus a network configuration) \mathcal{N}_j such that:

$$\sup_x |\mathcal{N}_j(x) - f_j(x)| \leq C_d \cdot \omega\left(f_j, \frac{1}{n^L}\right). \quad (23)$$

The global error of the vector-valued network is determined by the worst-case component error:

$$\|\mathcal{N} - f\|_{\infty, \text{vec}} = \sup_x \|\mathcal{N}(x) - f(x)\|_{\infty} \quad (24)$$

$$= \sup_x \max_j |\mathcal{N}_j(x) - f_j(x)| \quad (25)$$

$$= \max_j \left(\sup_x |\mathcal{N}_j(x) - f_j(x)| \right). \quad (26)$$

Substituting the scalar bounds:

$$\|\mathcal{N} - f\|_{\infty, \text{vec}} \leq \max_j \left(C_d \cdot \omega\left(f_j, \frac{1}{n^L}\right) \right) = C_d \cdot \max_j \omega\left(f_j, \frac{1}{n^L}\right). \quad (27)$$

This completes the proof. \square

C. Supplemental Data For Experiment 2

C.1. Experiment Setup: Gradient Dynamics in Reduced-Width Networks

To verify that the gradient stability observed in our primary results is an intrinsic property of the Bernstein basis rather than an artifact of architectural width, we extended the analysis of Section 5.2 to a constrained configuration. We trained a Fully Connected Network on the HIGGS dataset with the same depth ($L = 50$) but reduced the width by half ($W = 50$).

As illustrated in Figures 7 and 8, the results are strikingly consistent with our 100×50 experiments. DeepBern-Net maintains a dead neuron ratio significantly lower than all other baselines, preserving a high degree of connectivity despite the reduced capacity. Furthermore, the derivative profile remains smooth and strictly bounded, contrasting with the high-frequency fluctuations and signal decay observed in ReLU and its variants. This consistency across different width scales underscores the robustness of the Bernstein-based gradient persistence and confirms that our stabilization algorithm (Algorithm 1) effectively prevents “dead zones” even in resource-constrained architectures.

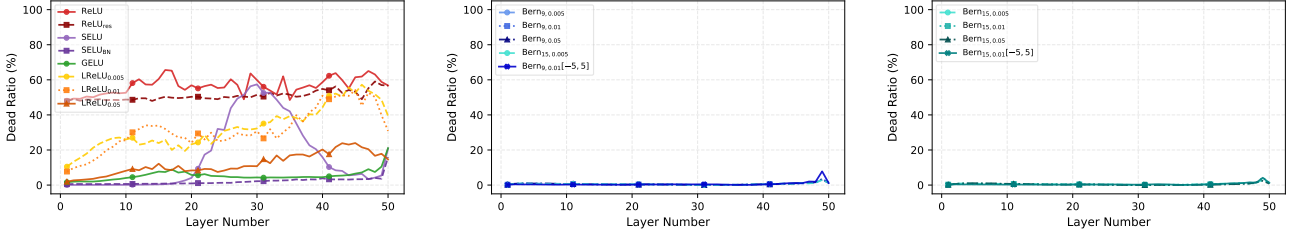


Figure 7. Dead Neuron Ratio comparison across activation functions on the NN architecture 50×50 on **HIGGS** dataset with the activation functions: ReLU, ReLU_{res}, SELU, SELU_{BN}, GELU, LReLU_{0.005}, LReLU_{0.01}, LReLU_{0.05} against (left) Bern_{9,0.01} $[-5, 5]$, Bern_{15,0.01} $[-5, 5]$, (middle) Bern_{9,0.005}, Bern_{9,0.01}, Bern_{9,0.05}, Bern_{9,0.01} $[-5, 5]$, and (right) Bern_{15,0.005}, Bern_{15,0.01}, Bern_{15,0.05}, Bern_{15,0.01} $[-5, 5]$. The y-axis shows the average dead neuron percentage over the last epoch for a layer in logarithmic scale vs. the layer number.

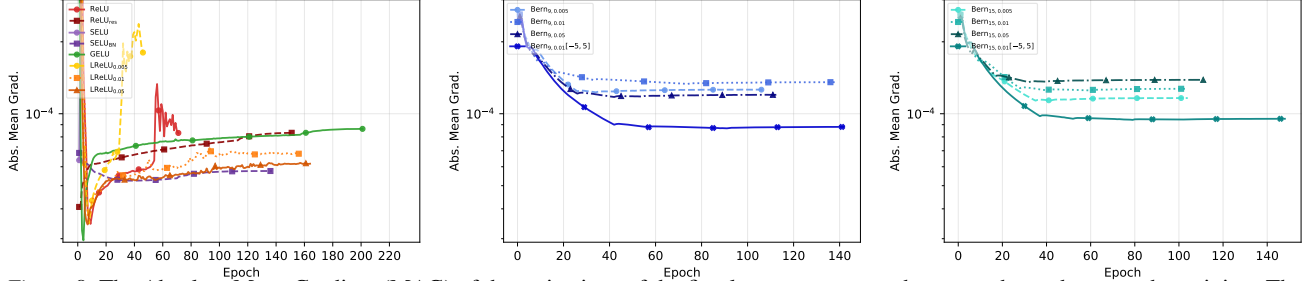


Figure 8. The Absolute Mean Gradient (MAG) of the activations of the first layer over an epoch vs. epoch number over the training. The comparison across activation functions on the NN architecture 50×50 for the dataset **HIGGS** with the activation functions: ReLU, ReLU_{res}, SELU, SELU_{BN}, GELU, LReLU_{0.005}, LReLU_{0.01}, LReLU_{0.05} against (left) Bern_{9,0.01} $[-5, 5]$, Bern_{15,0.01} $[-5, 5]$, (middle) Bern_{9,0.005}, Bern_{9,0.01}, Bern_{9,0.05}, Bern_{9,0.01} $[-5, 5]$, and (right) Bern_{15,0.005}, Bern_{15,0.01}, Bern_{15,0.05}, Bern_{15,0.01} $[-5, 5]$. The y-axis is in logarithmic scale.

C.2. Heatmaps of Dead Neuron Ratios

To provide a comprehensive view of network connectivity, we visualize the dead neuron ratio across both the depth of the architecture (layers) and the duration of optimization (epochs) using heatmaps. This allows us to observe the stability of the gradient flow dynamics throughout the entire training trajectory. Figures 9-10 illustrate these dynamics for the 100×50 HIGGS and MNIST configurations, as well as the 50×50 HIGGS variant.

- **DeepBern-Nets Persistence:** The heatmaps for DeepBern-Nets reveal a consistent “active zone” (low dead ratio) that persists across all layers and epochs. Unlike baselines that often start with active gradients but quickly *calcify* into dead zones, the Bernstein architecture maintains a stable, low-sparsity signature from initialization to convergence.
- **Contrast with Baselines:** These visualizations corroborate the findings in Experiment 2, showing that our architecture avoids the catastrophic *clogging* seen in SELU and the volatile, fluctuating patterns characteristic of ReLU and Leaky ReLU.
- **Scale Invariance:** The heatmaps for the 50×50 configuration are qualitatively identical to the 100×50 results, further confirming that our gradient-anchoring mechanism is robust to changes in network width and data distribution.

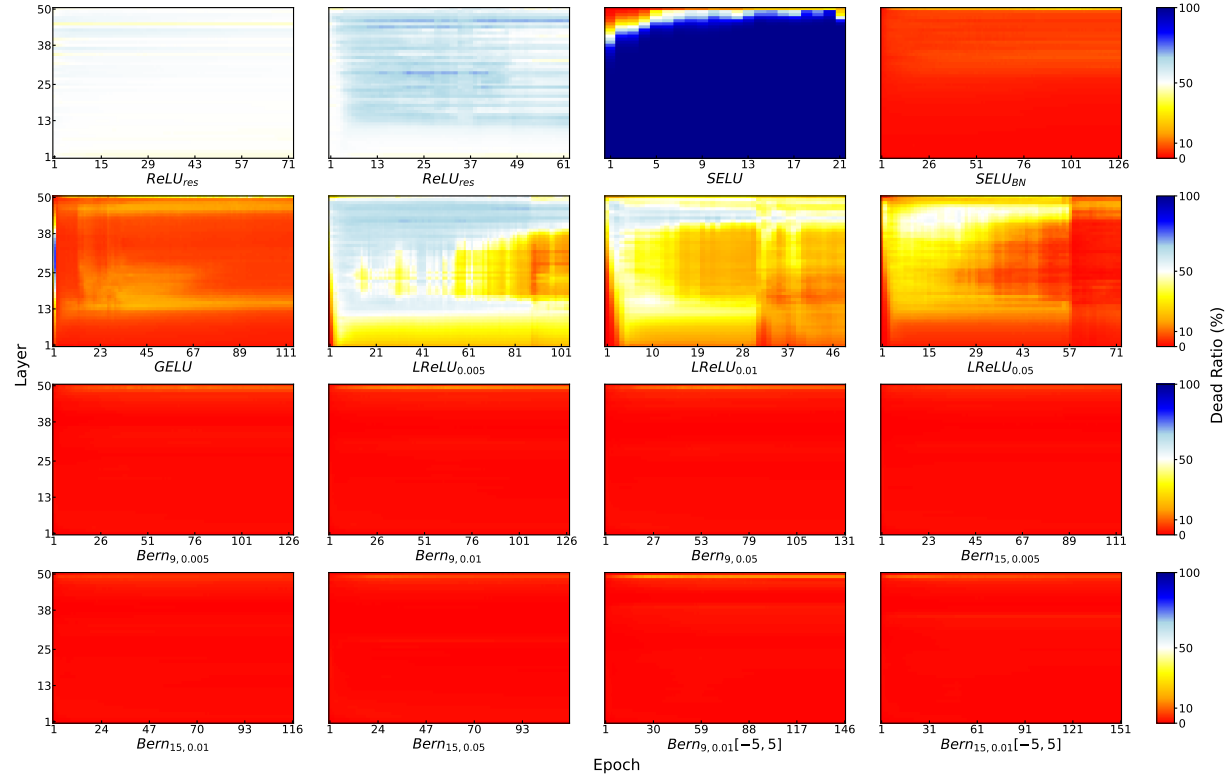


Figure 9. Spatio-temporal heatmaps of dead neuron ratios ($|\sigma'(z)| < 10^{-7}$) across training epochs and network depth for the 100×50 network trained on the HIGGS dataset. Warm colors indicate high sparsity (dead zones).

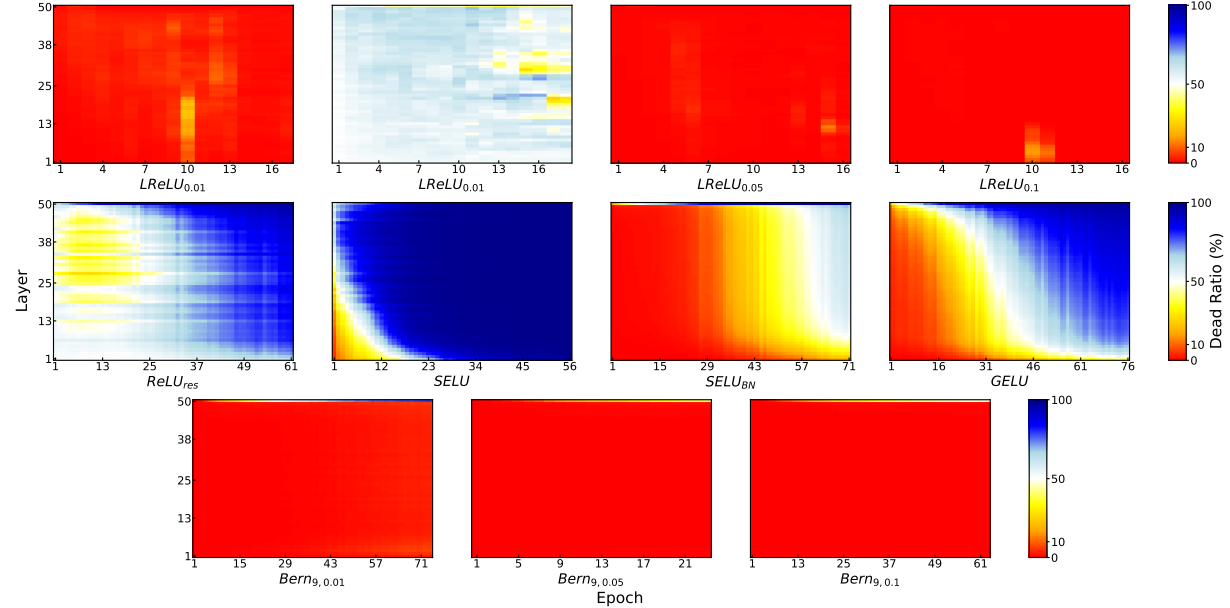


Figure 10. Spatio-temporal heatmaps of dead neuron ratios ($|\sigma'(z)| < 10^{-7}$) across training epochs and network depth for the 100×50 network trained on the MNIST dataset. Warm colors indicate high sparsity (dead zones)

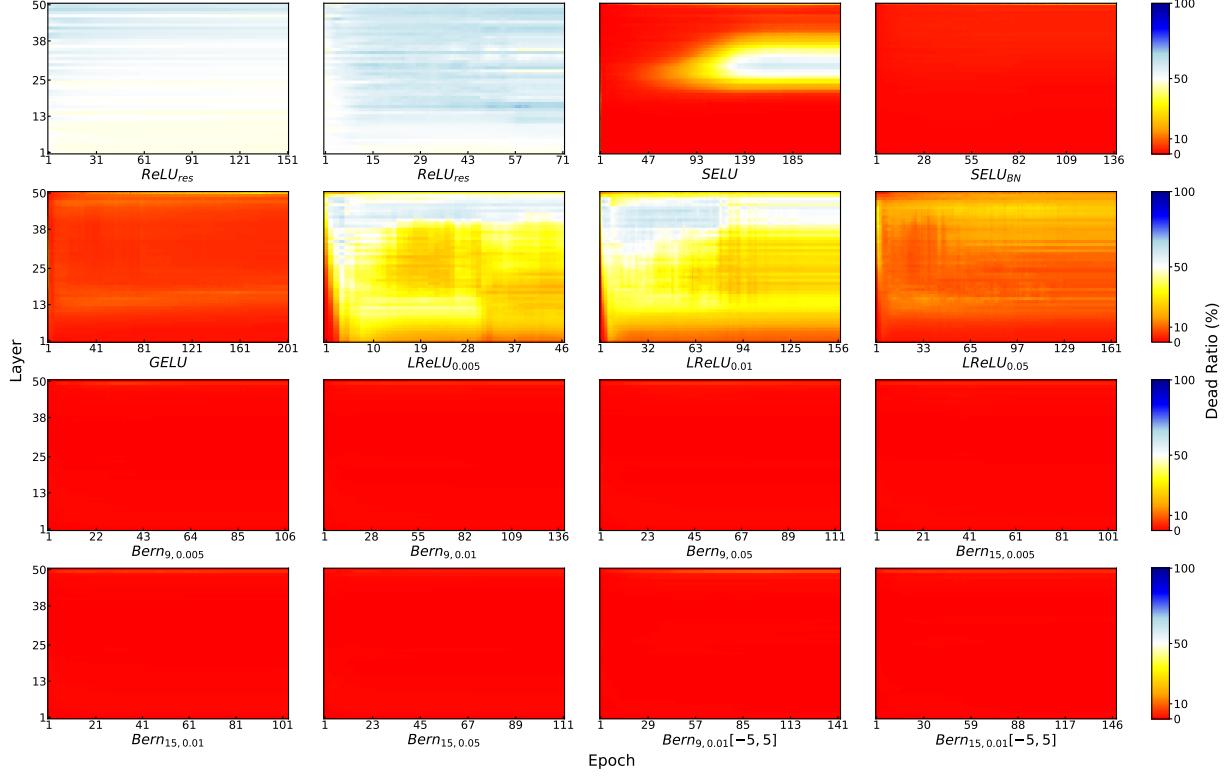


Figure 11. Spatio-temporal heatmaps of dead neuron ratios ($|\sigma'(z)| < 10^{-7}$) across training epochs and network depth for the 50×50 network trained on the HIGGS dataset. Warm colors indicate high sparsity (dead zones)

D. Supplemental Data For Experiment 3

Table 3 demonstrates that even with a reduced architecture of 50×50 , the DeepBern-Net (Order 15) achieves a lower training loss than the full-width 100×50 ReLU baseline. Furthermore, Table 2 compares Bernstein networks against a standard $[300, 100]$ ReLU baseline on MNIST. Remarkably, a single-layer Bernstein network with only 150 neurons outperforms the deeper ReLU baseline. It is important to note that for these shallow MNIST experiments, we relaxed the strict monotonicity constraint, as the gradient vanishing issue is less critical in shallow regimes. These results align with our theory of approximation.

Table 2. Best training losses on MNIST for ReLU and Bernstein models across different layer configurations.

Exp #	Activation	Layers	Best Training Loss
1	ReLU	[300,100]	0.0014
2	Bern3	[300,100]	0.0003
3	Bern5	[300,100]	0.0002
4	Bern9	[300,100]	0.0001
6	Bern3	[150,50]	0.0009
7	Bern5	[150,50]	0.0017
8	Bern9	[150,50]	0.0003
10	Bern3	[200]	0.0045
11	Bern5	[200]	0.0025
12	Bern9	[200]	0.0006
14	Bern3	[150]	0.0054
15	Bern5	[150]	0.0012
16	Bern9	[150]	0.0003

Table 3. Best training losses on HIGGS for ReLU and Bernstein models across layer configurations.

Exp #	Activation	Layers	Best Training Loss
1	ReLU	100×50	0.4783
2	Bern _{9,0.005}	50×50	0.4796
3	Bern _{9,0.01}	50×50	0.4784
4	Bern _{15,0.005}	50×50	0.4743
5	Bern _{15,0.01}	50×50	0.4763